Refinement of the Geometry of the Retinal Binding Pocket in Dark-Adapted Bacteriorhodopsin by Heteronuclear Solid-State NMR Distance Measurements†

Michael Helmle,‡,§ Heiko Patzelt,‡,|| Andreas Ockenfels,⊥ Wolfgang Gärtner,‡,⊥ Dieter Oesterhelt,‡ and Burkhard Bechinger*,‡

Max-Planck-Institut für Biochemie, Am Klopferspitz 18A, 82152 Martinsried, Germany, and Max-Planck-Institut für Strahlenchemie, Stiftstrasse 34-36, 45470 Mülheim an der Ruhr, Germany

Received March 23, 2000; Revised Manuscript Received May 24, 2000

ABSTRACT: The bacterial proton pump bacteriorhodopsin (BR) is a 26.5 kDa seven-transmembrane helical protein. Several structural models have been published at ≥1.55 Å resolution. The initial *cis*−*trans* isomerization of the retinal moiety involves structural changes within <1 Å. To understand the chromophore−protein interactions that are important for light-driven proton transport, very accurate measurements of the protein geometry are required. To reveal more structural details at the site of the retinal, we have, therefore, selectively labeled the tryptophan side chains of BR with ^{15}N and metabolically incorporated retinal, ^{13}C-labeled at position 14 or 15. Using these samples, heteronuclear distances were measured with high accuracy using SFAM REDOR magic angle spinning solid-state NMR spectroscopy in dark-adapted bacteriorhodopsin. This NMR technique is applied for the first time to a high-molecular mass protein. Two retinal conformers are distinguished by their different isotropic 14-^{13}C chemical shifts. Whereas the C14 position of 13-*cis*-15-*syn*-retinal is 4.2 Å from [*indole*-^{15}N]Trp86, this distance is 3.9 Å in the all-*trans*-15-*anti* conformer. This latter distance allows us to check on the details of the active center of BR in the various published models derived from X-ray and electron diffraction data. The experimental approach and the results reported in this paper enforce the notion that distances between residues of a membrane protein binding pocket and a bound ligand can be determined at subangstrom resolution.

The intrinsic membrane protein bacteriorhodopsin (BR)[1] of the archaeon *Halobacterium salinarum* acts as a light-driven proton pump. Due to its facile preparation, its remarkable stability, and its abundant presence in the cell membrane of *H. salinarum*, an impressive amount of structural and functional information about BR has been collected. It has thus become a model system for the protein family of retinal-containing, membrane-embedded photoreceptors of halobacteria, and even is assumed as a paradigm for ligand-activated receptors which have a high level of interest in pharmacological research. Considerable progress has recently been made in the determination of the high-resolution structure of BR using X-ray or electron diffraction techniques which have arrived at a resolution of ≥1.55 Å (*1*−*5*). Such detailed pictures have enabled the identification of various amino acids involved in the proton transport process and also show the overall structure of the retinal chromophore and the architecture of the chromophore binding pocket. A precise description of the interactions between retinal and the surrounding amino acids, or of the conformational changes during the light- to the dark-adapted state of the chromophore, which cover only a fraction of an angstrom is, however, still not possible on the basis of the crystal structures. More accurate structural data of the core region of this protein, in particular in the retinal environment, are, therefore, essential for the understanding of the fundamental processes of light-driven vectorial proton translocation.

NMR spectroscopy provides an alternative route for obtaining structural information about membrane proteins which can extend well into the subangstrom range. This technique can, therefore, supply supporting information which helps to fine-tune structural models from other techniques. Whereas solution NMR spectroscopy works well with small globular proteins or protein-detergent complexes that exhibit fast rotational correlation times (*6*, *7*), solid-state NMR spectroscopy provides structural information about samples that are immobilized on the NMR time scale. Solid-state NMR spectroscopy, which does not require the high degree of sample order necessary for diffraction techniques, has been applied to purple membranes in several previous studies (reviewed in refs *8* and *9*).

† The work of D.O. was supported by the Deutsche Forschungsgemeinschaft (Sonderforschungsbereich 533).

* To whom correspondence should be addressed. Telephone: +49 89 8578-2466. Fax: +49 89 8578-2876. E-mail: bechinge@biochem.mpg.de.

‡ Max-Planck-Institut für Biochemie.

§ Present address: IXOS Software GmbH, Technopark Neukeferloh, Bretonischer Ring 12, 85630 Grasbrunn, Germany.

|| Present address: Sultan Qaboos University, P.O. Box 36, 123 Al-Khod, Oman.

⊥ Max-Planck-Institut für Strahlenchemie.

[1] Abbreviations: BR, bacteriorhodopsin; CD, circular dichroism; CP, cross polarization; DBU, 1,8-diazabicyclo[5.4.0]undec-7-ene; DIBAH, diisobutylaluminum hydride; HPLC, high-performance liquid chromatography; MAS, magic angle spinning; NMR, nuclear magnetic resonance; NOE, nuclear Overhauser enhancement; PDB, Brookhaven Protein Data Bank; PM, purple membrane; PSB, protonated Schiff base; REDOR, rotational-echo double-resonance; RF, radio frequency; SFAM, simultaneous frequency and amplitude modulation.

10.1021/bi0006666 CCC: $19.00
Published on Web 07/28/2000

Two fundamentally different approaches can be used to record high-resolution solid-state NMR spectra. First, measurements have been performed on static samples that are uniaxially aligned with respect to the magnetic field direction. The orientational dependence of nuclear interactions with respect to the magnetic field direction has provided angular constraints for the retinal moiety in bacteriorhodopsin with respect to the purple membrane normal (*8*, *10*). Similarly, oriented ^{2}H, ^{15}N, and ^{13}C solid-state NMR spectroscopy has been used to determine the three-dimensional backbone and side chain structures of gramicidin A at atomic resolution (*11*), and to investigate the topological equilibria of membrane-active peptide antibiotics (*12*).

Second, magic angle spinning (MAS) NMR uses mechanical rotation of the samples around the magic angle ($\Theta = 54.7°$) to obtain high-resolution solid-state NMR spectra also in materials without any preferential macroscopic alignment. This approach ensures efficient averaging of nuclear interaction anisotropies. The spectra, therefore, exhibit isotropic chemical shift values similar to those recorded from solutions. Using solid-state NMR spectroscopy, important information about the chemical environment of retinal as well as about the amino acid backbone or side chains in BR has been obtained (reviewed in ref *9*; for more recent applications, see refs *13*−*15*). This approach requires the specific or selective isotopic labeling of amino acids or the retinal moiety with ^{13}C or ^{15}N. Furthermore, magic angle spinning sideband intensities were analyzed to extract the three main tensor elements which characterize the chemical shift anisotropy and thereby provide more detailed structural information than the isotropic value alone (*16*, *17*). Using solid-state NMR spectroscopy, the chemical shift anisotropies and the isotropic chemical shifts confirm the resonance Raman data which reveal a 15-*syn* conformation of the C═N double bond of retinal in BR_{548},[2] but a 15-*anti* conformation in BR_{568} (*18*, *19*). Similarly, a detailed chemical shift analysis indicates a 6-*s-trans* conformation of the retinal chromophore (*20*, *21*).

Since magic angle spinning also abolishes dipolar couplings and thereby eliminates valuable distance information, MAS NMR experiments have been designed which specifically interfere with rotational averaging of dipolar interaction terms (*22*, *23*). These experiments, at the same time, keep with the averaging of other anisotropic interactions such as chemical shifts. The local dipolar field strength is related to the distance between the nuclei, and measurements of homonuclear or heteronuclear dipolar interactions make accessible highly accurate geometrical information in non-ordered condensed matter. Distances measured by rotational resonance NMR spectroscopy between two ^{13}C-labeled positions within the retinal confirm the 6-*s-trans* conformation (*24*, *25*). In addition, distance determinations between the [14-^{13}C]retinal moiety and [ϵ-^{13}C]Lys 216 reveal the presence of both 13-C *cis*, C═N *syn* and all-*trans*, C═N *anti* configurations in dark-adapted BR (*26*). Furthermore, to investigate the alignment of the retinal moiety with respect to the membrane normal, [18-C-$^2H_3$]retinal has been synthesized and incorporated into bacterioopsin. The thus obtained purple membranes have been oriented on glass plates, rotated around the magic angle, and investigated by magic angle-oriented sample spinning ^{2}H NMR spectroscopy (*27*). This approach utilizes the improved sensitivity and resolution of magic angle spinning NMR spectroscopy without losing orientational information.

Table 1: Distances between Retinal Carbons and Indole N Atoms in the Side Chains of Tryptophan 86 or Tryptophan 182 in High-Resolution X-ray and Electron Microscopic Structures

ref	method	resolution (Å)	W86−C14	W182−C14
5[a]	X-ray	1.55	3.44	5.86
3[a]	X-ray	1.9	3.62	5.83
28	X-ray	2.3	3.53	6.24
29[b]	X-ray	2.5	3.83	6.14
4	X-ray	2.9	3.65	5.88
30	EM	3.0	3.58	6.02
31[a]	X-ray	3.5	3.83	5.94
1[c]	EM	3.5/4.3	4.03	6.08
this study, all-*trans* (BR_{568})[d]			3.9	

[a] Light-adapted BR has been investigated. [b] The conformation of the chromophore in the crystal or electron microscopic structure has been adjusted as the all-*trans* conformation. [c] The retinal conformation is based on ref *32*. [d] The statistical error of the NMR distance measurements is less than ±0.3 Å; see the text for details.

The work presented in this paper uses structural information available from X-ray and electron diffraction measurements to more specifically design experiments that provide selected but accurate information about the distance between the retinal and the proteinaceous binding pocket. The structural models indicate that the side chain of Trp86 is in proximity to the 14 or 15 position of retinal (Table 1). ^{15}N isotopic labels were, therefore, selectively incorporated into the tryptophan side chains of the protein moiety. The retinal was chemically prepared, specifically labeled with ^{13}C, and metabolically incorporated into the protein during the biogenesis of purple membranes of a retinal deficient *H. salinarum* strain. Thereafter, distances between the retinal and the tryptophan side chain were measured using the recently developed solid-state NMR technique SFAM REDOR (*33*). To our knowledge, we present the first example where this novel technique has been combined with advanced labeling methods to solve the specific problems that are associated with structural studies of large proteins. As an advantage over the X-ray structure information, which is obtained from low-temperature samples, all of the experiments presented here were performed at ambient temperatures where the protein is capable of actively converting light into chemical energy. When compared to previous intramolecular NMR distance measurements within a ligand or a prosthetic group, this study reveals connectivities between retinal and amino acid side chains which on average extend further apart considerably. The problems encountered in this study, therefore, effectively represent the situation when the geometrical interactions of a ligand in the binding pocket of a receptor protein are to be tested (*34*). By a similar solid-state NMR approach, the distance between Trp182 and position 20 of retinal under conditions of illumination has recently been measured (*35*).

[2] On the basis of previous reconstitution and solid-state NMR experiments, this conformational state is often assigned as BR_{555} in the literature (*9*, *23*, *52*). The mixture of conformers in dark-adapted BR exhibits its maximum at 558 nm. We prefer, however, to use the widely accepted nomenclature and assign the 13-*cis*, 15-*syn* conformer with BR_{548}.

MATERIALS AND METHODS

Synthesis of [14-^{13}C]- and [15-^{13}C]Retinal. Retinals labeled with ^{13}C at position 14 or 15 were synthesized starting from β-ionone. Wittig−Horner reaction of β-ionone and (2-diethylphosphonato)acetonitrile, followed by reduction of the formed nitrile compound (DIBAH, toluene), yielded the C_{15}-aldehyde (β-ionylidene acetaldehyde). Aldole condensation of this aldehyde with acetone yielded the "C_{18}-ketone" [5-(β-ionylidene)pent-3-en-2-one] (*36*). C_{18}-Ketone was subjected to an aldole reaction with 1- or 2-^{13}C-labeled acetonitrile, followed by acetylation (by acetic anhydride) of the resulting alcohol, and double bond formation (removal of acetic acid) employing DBU to yield the target retinals (*37*). The all-*trans* isomers of the ^{13}C-labeled retinals were purified by HPLC and characterized by ^{1}H NMR and mass spectrometry. The spectroscopic data were in full agreement with the values reported in the literature.

Preparation of Purple Membranes. Oxoid bacteriological peptone L34 (56 g) was depleted from tryptophan by heating to reflux in 6 M HCl (0.6 L) for 48 h. The product was lyophilized, taken up in water, neutralized with NaOH, treated with activated charcoal (10 g), filtered, and lyophilized again. With this preparation, a halobacterial standard medium (*38*) was prepared and contained the following compounds (amount per liter of H_2O): peptone (10 g), NaCl (250 g), $MgSO_4 \cdot 7H_2O$ (20 g), trisodium citrate$\cdot 2H_2O$ (3 g), and KCl (2 g). The pH was adjusted to 7.0, and 102 mg/L [*indole*-^{15}N]Trp (Promochem, Wesel, Germany) was added prior to sterilization.

The retinal-negative strain *H. salinarum* JW5 (*38*) was grown in this medium for 10 days at 37 °C, in 700 mL cultures on a rotary shaker at 100 rpm. [14-^{13}C]- or [15-^{13}C]retinal (30 mM 2-propanol) was added on days 3 (350 μL), 4, 5, and 6 (100 μL each, per culture). The purple membranes were isolated and purified as described previously (*6*). From a total fermentation volume of 5.6 L, 110 mg of labeled PM was obtained. The buffered suspension was centrifuged at 48000*g* for 30 min. The pellet was transferred into a 4 mm boron nitride MAS rotor, followed by tabletop centrifugation to ensure dense packing within the rotor. After loading of the rotor was complete, excess water was removed.

All NMR experiments were carried out at ambient temperature using a Bruker DMX400 NMR spectrometer operating at 9.4 T. The sample was inserted into a commercial triply tuned 4 mm MAS probe, and the rotor speed was stabilized at 5000 ± 3 Hz with the help of a commercial spinning speed controller. Before distance measurements were performed, one-dimensional (1D) CP/MAS spectra were acquired for at least 1 h to allow for complete relaxation of bacteriorhodopsin into the dark-adapted state. For every dephasing delay, a SFAM REDOR (*33*) and a reference experiment without dipolar recoupling were recorded back to back (*39*). This approach allows us to separate the dipolar modulation of signal intensities from other contributions such as transverse relaxation. The SFAM pulses were implemented by directly generating "shaped pulse" files using a C program. These are read by the Bruker pulse programmer prior to execution. The experiments were run in a 1D acquisition mode. Since the pulse programming unit does not support fast frequency switching within a pulse, the frequency modulation was incorporated via TPPI phase modulation (*40*, *41*). The following experimental parameters were applied: 1.2 ms cross polarization pulses at B_1 field strengths of 50 kHz, SFAM frequency modulation at 33 kHz, a proton decoupling field of 85 kHz, a 180° pulse length of the ^{13}C and ^{15}N channels of 8 and 16 μs, respectively, a 41 ms acquisition time using 4K data points, a 3 s recycle delay, and 20 000 transients. Before Fourier transformation, an exponential apodization function (line broadening equivalent to 20 Hz) was applied. The effective recoupling factor was calibrated using [^{15}N]alanine under similar experimental conditions ($\gamma = 0.75$).

The ^{13}C NMR chemical shifts were calibrated against the $^{13}C_\alpha$ resonance of alanine (50.5 ± 0.5 ppm with respect to a tetramethylsilane chemical shift scale). The peak intensities were determined by fitting the peaks to a Lorentzian line shape. To determine distances, the signal intensities were then fitted to a REDOR curve generated by a MATHEMATICA program (www.wolfram.co.uk) based on the analytical expression and code of Mueller (*42*). Only one variable, namely, the strength of the efficient dipolar coupling, needs to be adjusted. Internuclear distances were calculated according to the relation $D(r_{ij}) = (\mu_o h/16\pi^3)(\gamma_i\gamma_j/r_{ij}^3)$. Statistical variations in the recorded intensities were used to estimate the errors for the calculated ^{15}N−^{13}C dipolar coupling and the internuclear distance. Systematic errors can arise from the calibration of the recoupling factor. Their influence on the evaluation of internuclear distances was estimated to remain <0.15 Å. Possible interference from other nearby ^{15}N nuclei was also considered. In cases where the homonuclear interactions between the two S-spins can be neglected (the indole nitrogens of residues 86 and 182 are approximately 9 Å apart), the total dephasing of the system is a product of cosine terms containing the heteronuclear dipolar interactions and the relative alignments of interaction vectors (*43*). In the published structures, the side chain of Trp86 is significantly closer to the C14 position of the retinal than either Trp182 or any other tryptophan residue (Table 1). When the dipolar interaction that arises from a second pair of ^{15}N−^{13}C nuclei (distance of approximately 6 Å) is not explicitly taken into consideration, a quantitative analysis which assumes a single interaction pair slightly underestimates the true distance. Due to the r^{-3} dependence of dipolar interactions, this effect will not affect our final conclusions. From the REDOR reference experiment (i.e., without the SFAM recoupling pulse on the ^{15}N channel), transverse relaxation rates were determined. T_2 relaxation times were compared to the resonance line width at half-height using the relationship $\Delta\nu = 1/(\pi T_2)$.

RESULTS

Figure 1 shows the proton-decoupled ^{13}C MAS solid-state spectrum of [[*indole*-^{15}N]tryptophan,[14-^{13}C]retinal]BR. The resonances at 122.3 and 110.7 ppm exhibit enhanced intensities when compared to those of natural abundance bacteriorhodopsin. These resonances are, therefore, assigned to the all-*trans* and 13-*cis* conformations of retinal, respectively, which both exist in dark-adapted BR (*18*, *19*). The ratio of all-*trans*/13-*cis* which was calculated from the integrals of the ^{13}C resonances shown in Figure 1 is approximately 40/60 and agrees well with previously published ratios of the two dark-adapted conformations of

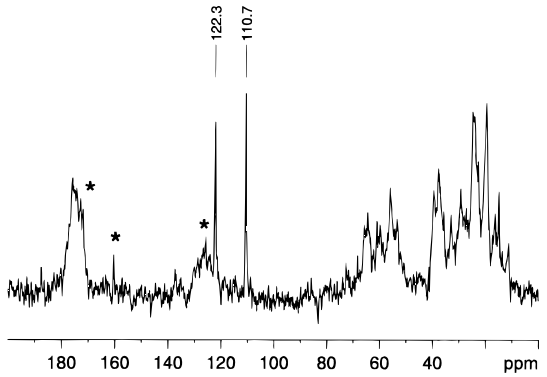

FIGURE 1: Proton-decoupled ^{13}C CP/MAS spectrum of dark-adapted [[*indole*-^{15}N]tryptophan,[14-^{13}C]retinal]bacteriorhodopsin recorded at ambient temperature and at a spinning speed of 5000 Hz. The selectively introduced ^{13}C label at the C14 position of the retinylidene chromophore gives rise to two sharp peaks (110.7 and 122.3 ppm) which can be assigned to different conformations in dark-adapted BR, namely, BR_{548} and BR_{568}. Signals marked with an asterisk indicate spinning side bands.

Table 2: Summary of the NMR-Derived Dipolar Couplings and Calculated Distances for [[*indole*-^{15}N]tryptophan,[14-^{13}C]retinal]Bacteriorhodopsin

	BR_{568} (all-*trans*)	BR_{548} (13-*cis*)
chemical shift (ppm)	122.3	110.7
dipolar coupling (Hz)	50	41
$^{15}N-^{13}C$ distance (Å)	3.9	4.2
T_2 relaxation time (ms)	18.4	27.5

bacteriorhodopsin BR_{568}/BR_{548} (33/67 to 50/50) (*6*, *19*, *44*, *45*). It is noteworthy that the observed line broadening can be fully ascribed to T_2 relaxation (Table 2). The narrow lines are, therefore, indicative of fast averaging of structural inhomogeneities at room temperature and at full hydration.

Figure 2 exhibits the relative decrease in the signal intensities of [14-^{13}C]retinal as a function of dephasing time due to its interactions with ^{15}N-labeled tryptophan (REDOR effect). The decay in signal amplitude is normalized according to $(S_o - S)/S_o$, where S is the proton-decoupled ^{13}C signal intensity in the presence of the recoupling pulse switching the $^{13}C-^{15}N$ dipolar interactions active, and S_o is the signal intensity in the reference without the recoupling pulses (*33*, *39*). The observed modulation of signal amplitudes is a function of the effective dipolar coupling. Although transverse relaxation allows the comparison of signal intensities only within a period of 30 ms, the observed initial oscillation is very sensitive to the strength of the effective dipolar interaction and allows us to deduce highly accurate internuclear distances. The continuous lines also shown in Figure 2 represent the best fit of the experimental values of the signals of BR_{568} and BR_{548}. The resulting distances are 3.9 and 4.2 Å, respectively. When the experimental values and the SFAM REDOR decay curves of all-*trans*- and 13-*cis*-retinal in BR are compared to each other, significant differences are observed. These data, therefore, indicate that the statistical error is <0.3 Å.

In a second set of experiments, BR-containing [15-^{13}C]-retinal together with [*indole*-^{15}N]tryptophan was prepared and investigated by solid-state NMR spectroscopy using the SFAM REDOR technique. Although considerably less of this protein was available and the signal-to-noise ratios of these spectra were limiting for the accuracy of the analysis, the distances measured for this compound were 4.2 and 3.1 Å (±1 Å) for BR_{568} (159.7 ppm) and BR_{548} (163.2 ppm), respectively.

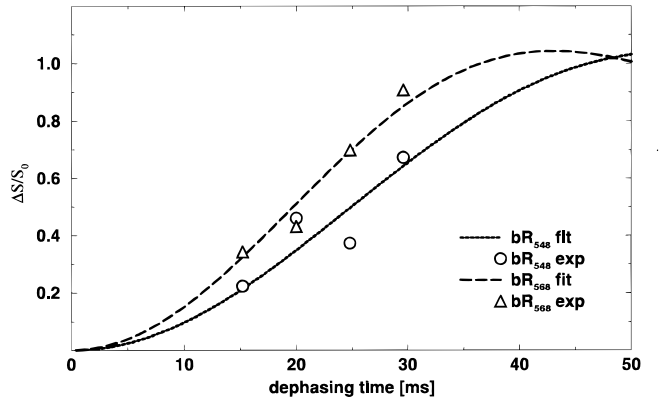

FIGURE 2: Resulting SFAM REDOR curves for [[*indole*-^{15}N]-tryptophan,[14-^{13}C]retinal]bacteriorhodopsin. Plotted is the normalized SFAM REDOR signal $\Delta S/S_o$, where ΔS is the difference between the reference experiment and the SFAM REDOR experiment performed at the same refocusing time. The experimental error for individual data points is estimated to be ±0.15 and ±0.1 for BR_{568} and BR_{548}, respectively.

DISCUSSION

The challenge of this investigation was to measure an approximately 40 Hz dipolar coupling in an experiment where the dipolar dephasing competes with transverse relaxation processes (Table 2). At the same time, the large size of the BR molecule results in a low molar amount of protein even though sufficient material is available to ensure a high filling factor of the coil. To obtain highly accurate data, it was, therefore, essential to optimize the NMR experiments, including the concentration of most signal intensities in the MAS center bands. This can be achieved by fast spinning speeds. Fast magic angle spinning of the sample also ensures high resolution in the chemical shift dimension. As the rotational velocity is limited by the length of the finite π-pulses of the classical REDOR experiment (*39*), a recently proposed development was used which achieves dipolar recoupling by a continuously applied simultaneous modulation of the frequency and amplitude (SFAM) of the ^{15}N radio frequencies (*33*). This technique at the same time ensures a high recoupling efficiency of the heteronuclear dipolar interaction, and thereby eases problems that result from RF field inhomogenieties in real NMR sample coils. SFAM REDOR solid-state NMR spectroscopy has previously been used during the investigation of the 15-amino acid peptide gramicidin M in lipid bilayers (*46*). Since up to now only low-molecular mass samples had been used, the application of this technique to BR, selectively and specifically labeled with ^{15}N and ^{13}C, respectively, introduces a new quality in this type of solid-state NMR structural investigations.

Distances between retinal position 14 or 15 and tryptophan 86 were measured as these atoms are located well within the proton conductive pathway of bacteriorhodopsin. In addition, the tryptophan side chain modulates the electronic properties of retinal by $\pi-\pi$ electron interactions and also has been suggested to be part of the complex counterion of the protonated retinal Schiff base (*1*, *47*). This extended

counterion is characterized by a comparatively low hydrogen bonding interaction with the Schiff base and ensures a fast connectivity to the extracellular medium due to the involvement of water molecules (*48*, *49*). The indole N of Trp86 is in proximity to Asp212 and Asp85 (*1*−*5*), which are also part of the Schiff base counterion. Furthermore, Asp85 acts as a proton acceptor in the translocation machinery. Tryptophan side chain chemical shifts (of so far unassigned residues) have previously been investigated by solid-state (*50*) and multidimensional solution NMR spectroscopies (*6*).

Table 1 compares the interatomic distances derived from our direct SFAM REDOR measurements with the corresponding distances from high-resolution X-ray or electron microscopy structures. It is evident that, although high-quality and -resolution structures are available, considerable differences exist between the published data. Clearly, the structural models deposited in databases are derived from diffraction patterns of ≥1.55 Å resolution. These atomic coordinates are, therefore, not as accurate as the individual models tend to suggest (Table 1). Although it is difficult to accurately determine the variance of structural models obtained from diffraction data at every protein site, this error is certainly smaller than the diffraction limit for the retinal binding pocket in BR. To obtain better estimates of the accuracy of these models, the distances presented in this paper could, for example, be used as an additional constraint and checked against the electron density map in molecular modeling calculations.

Highly accurate NMR distance measurements indicate that the local environment of the retinal binding pocket at ambient temperatures seems to be better represented by some of the structural models deposited in the Brookhaven Protein Data Bank (Table 1). For the NMR results, a statistical error of 0.2 Å which is biased by potential systematic deviations (as discussed in Materials and Methods) should be taken into account during this comparison. Therefore, of the diffraction structures listed in Table 1, those with distances of ≥3.6 Å are in agreement with our NMR result. Whereas some structural models are characterized by distances well within this range, the remaining ones deviate marginally. Nevertheless, only few structures perfectly agree with our SFAM REDOR NMR data. This, however, should not be taken as an indication of the overall quality of other structures. It is very possible that other features, such as the extracellular and cytoplasmic regions of the proton channel, interhelical loops (*2*), the charges of aspartates (*1*, *30*), or BR-associated lipids (*1*, *3*−*5*), are better described by other models. When the limitations in resolution of the X-ray and electron microscopic data, the experimental errors of NMR distance measurements, and the differences in experimental conditions used during diffraction and NMR experiments are taken into account, any one of the structures listed in Table 1 is probably in accord with our NMR results. Similarly, NOE-based structure calculations of the retinal binding pocket agree well with the data presented in this paper (R. Kühne, B. Simon, H. Patzelt, D. Oesterhelt, and H. Oschkinat, unpublished). Interestingly, the largest differences arise when light-adapted protein reconstituted from lipid cubic phases is investigated at 100 K (*3*, *5*). Within the all-*trans* structures of BR, the possibility of small conformational differences depending on the presence of light, temperature, or other experimental conditions should also be taken into consideration. Previous CD spectroscopic investigations have, for example, revealed significant conformational alterations in BR during temperature cycling (*51*).

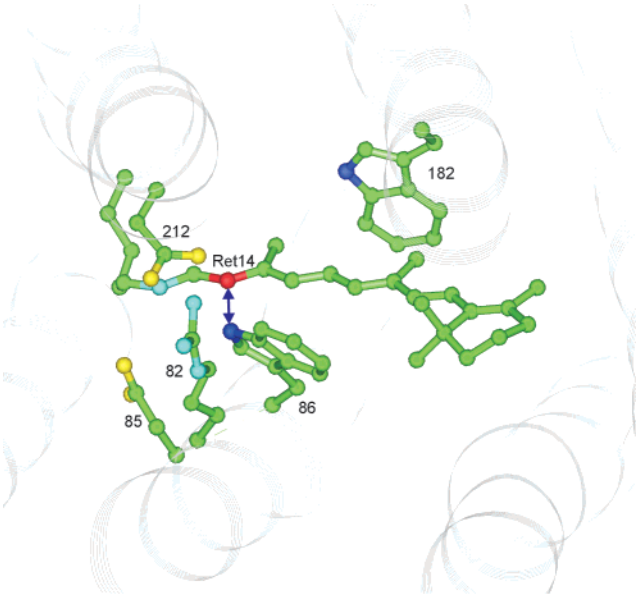

FIGURE 3: Binding pocket of retinal in BR with the accurate distance measured by solid-state SFAM REDOR NMR spectroscopy. The PDB structural model of Grigorieff et al. (*1*) was used. The retinal C14 position is shown in red and the indole nitrogen of Trp86 and Trp182 in dark blue; the nitrogen atoms of the Schiff base and Arg82 are shown in light blue and the oxygens of Asp85 and Asp212 in yellow.

Recently, an accurate solid-state NMR-derived distance of 3.7 Å between the C20 methyl group of all-*trans*-retinal and the Trp182 side chain has been presented (*35*). Our data and these data are in excellent agreement with some of the structural models which, therefore, seem to describe well the local environment of the retinal binding pocket in BR also at the experimental conditions used in the NMR studies (Table 1). For example, in the model of Grigorieff et al. (*1*), the distances between the retinal C14 atom and the indole nitrogen of Trp86 (4.0 Å) or retinal-C20 and Trp182 (3.7 Å) agree with the NMR-derived distances. A sketch of the binding pocket of BR is depicted in Figure 3.

When the SFAM REDOR decay curves of BR_{548} and BR_{568} are compared to each other, significant differences are observed (Figure 2). This is in agreement with the occurrence of *cis*−*trans* isomerizations of the retinal chromophore at the 13 and 15 positions. These have been shown to occur by resonance Raman experiments (*18*), NMR chemical shift analyses (*19*), and rotational resonance distance measurements (*26*). Interestingly, the appearance of both chromophore isomers is averaged in many crystalline samples (*2*, *4*, *29*).

The distances measured within the active site of the protein and the technology presented in this study provide important information which allows us to select those among the conformational models based on X-ray or EM diffraction analyses that best describe the core region of the bacteriorhodopsin proton pump under nearly physiological conditions. When the presence of two conformers of the chromophore in dark-adapted bacteriorhodopsin is taken into account, the concentration of each protein conformer corresponds to the molar amount of a homogeneous popu-

lation of >65 kDa proteins under comparable conditions. The results presented in this paper indicate that the direct determination of distances of several angstroms with sub-angstrom accuracy is possible in large membrane proteins by combining information from X-ray crystallography, EM diffraction, or homology modeling with advanced isotopic labeling schemes and up-to-date solid-state NMR technology. Provided that sufficient material for structural studies can be prepared, this approach will allow determination of the three-dimensional geometry of ligand binding pockets of other seven-transmembrane helical proteins of pharmacological interest such as G-protein-coupled receptors.

ACKNOWLEDGMENT

We are grateful to Lars-Oliver Essen for valuable discussions.

REFERENCES

1. Grigorieff, N., Ceska, T. A., Downing, K. H., Baldwin, J. M., and Henderson, R. (1996) *J. Mol. Biol. 259*, 393−421.
2. Kimura, Y., Vassylyev, D. G., Miyazawa, A., Kidera, A., Matsushima, M., Mitsuoka, K., Murata, K., Hirai, T., and Fujiyoshi, Y. (1997) *Nature 389*, 206−211.
3. Belrhali, H., Nollert, P., Royant, A., Menzel, C., Rosenbusch, J. P., Landau, E. M., and Pebay-Peyroula, E. (1999) *Structure 7*, 909−917.
4. Essen, L. O., Siegert, R., Lehmannn, W. D., and Oesterhelt, D. (1998) *Proc. Natl. Acad. Sci. U.S.A. 95*, 11673−11678.
5. Luecke, H., Schobert, B., Richter, H. T., Cartailler, J. P., and Lanyi, J. K. (1999) *J. Mol. Biol. 291*, 899−911.
6. Patzelt, H., Ulrich, A. S., Egbringhoff, H., Dux, P., Ashurst, J., Simon, B., Oschkinat, H., and Oesterhelt, D. (1997) *J. Biomol. NMR 10*, 95−106.
7. Pervushin, K., Riek, R., Wider, G., and Wüthrich, K. (1998) *J. Am. Chem. Soc. 120*, 6394−6400.
8. Watts, A., Ulrich, A. S., and Middleton, D. A. (1995) *Mol. Membr. Biol. 12*, 233−246.
9. Engelhard, M., and Bechinger, B. (1995) *Isr. J. Chem. 35*, 273−288.
10. Moltke, S., Nevzorov, A. A., Sakai, N., Wallat, I., Job, C., Nakanishi, K., Heyn, M. P., and Brown, M. F. (1998) *Biochemistry 37*, 11821−11835.
11. Cross, T. A. (1997) *Methods Enzymol. 289*, 672−696.
12. Bechinger, B. (1996) *J. Mol. Biol. 263*, 768−775.
13. Tuzi, S., Naito, A., and Saito, H. (1996) *Eur. J. Biochem. 239*, 294−301.
14. Tuzi, S., Yamaguchi, S., Tanio, M., Konishi, H., Inoue, S., Naito, A., Needleman, R., Lanyi, J. K., and Saito, H. (1999) *Biophys. J. 76*, 1523−1531.
15. Petkova, A. T., Hu, J. G. G., Bizounok, M., Simpson, M., Griffin, R. G., and Herzfeld, J. (1999) *Biochemistry 38*, 1562−1572.
16. Maricq, M. M., and Waugh, J. S. (1979) *J. Chem. Phys. 70*, 3300−3316.
17. Herzfeld, J., and Berger, A. E. (1980) *J. Chem. Phys. 73*, 6021−6030.
18. Smith, S. O., Myers, A. B., Pardoen, J. A., Winkel, C., Lugtenburg, J., and Mathies, R. A. (1984) *Proc. Natl. Acad. Sci. U.S.A. 81*, 2055−2059.
19. Harbison, G. S., Smith, S. O., Pardoen, J. A., Winkel, C., Lugtenburg, J., Herzfeld, J., Mathies, R., and Griffin, R. G. (1984) *Proc. Natl. Acad. Sci. U.S.A. 81*, 1706−1709.
20. Harbison, G. S., Mulder, P. P. J., Pardoen, H., Lugtenburg, J., Herzfeld, J., and Griffin, R. G. (1985) *J. Am. Chem. Soc. 107*, 4809.
21. Harbison, G. S., Smith, S. O., Pardoen, J. A., Courtin, J. M., Lugtenburg, J., Herzfeld, J., Mathies, R. A., and Griffin, R. G. (1985) *Biochemistry 24*, 6955−6962.
22. McDowell, L. M., and Schaefer, J. (1996) *Curr. Opin. Struct. Biol. 6*, 624−629.
23. Griffin, R. G. (1998) *Nat. Struct. Biol., NMR Suppl.*, 508−512.
24. Creuzet, F., McDermott, A., Gebhard, R., van der Hoef, K., Spijker-Assink, M. B., Herzfeld, J., Lugtenburg, J., Levitt, M. H., and Griffin, R. G. (1991) *Science 251*, 783−786.
25. Mcdermott, A. E., Creuzet, F., Gebhard, R., Vanderhoef, K., Levitt, M. H., Herzfeld, J., Lugtenburg, J., and Griffin, R. G. (1994) *Biochemistry 33*, 6129−6136.
26. Thompson, L. K., Mcdermott, A. E., Raap, J., van der Wielen, C. M., Lugtenburg, J., Herzfeld, J., and Griffin, R. G. (1992) *Biochemistry 31*, 7931−7938.
27. Glaubitz, C., Burnett, I. J., Gröbner, G., Mason, A. J., and Watts, A. (1999) *J. Am. Chem. Soc. 121*, 5787−5794.
28. Luecke, H., Richter, H. T., and Lanyi, J. K. (1998) *Science 280*, 1934−1937.
29. Pebay-Peyroula, E., Rummel, G., Rosenbusch, J. P., and Landau, E. M. (1997) *Science 277*, 1676−1681.
30. Mitsuoka, K., Hirai, T., Murata, K., Miyazawa, A., Kidera, A., Kimura, Y., and Fujiyoshi, Y. (1999) *J. Mol. Biol. 286*, 861−882.
31. Sato, H., Takeda, K., Tani, K., Hino, T., Okada, T., Nakasako, M., Kamiya, N., and Kouyama, T. (1999) *Acta Crystallogr., Sect. D 7*, 1251−1256.
32. Santarsiero, B. D., James, M. N. G., Mahendran, M., and Childs, R. F. (1990) *J. Am. Chem. Soc. 112*, 9416−9418.
33. Fu, R., Smith, S. A., and Bodenhausen, G. (1997) *Chem. Phys. Lett. 272*, 361−369.
34. Watts, A., Burnett, I. J., Glaubitz, C., Grobner, G., Middleton, D. A., Spooner, P. J. R., and Williamson, P. T. F. (1998) *Eur. Biophys. J. 28*, 84−90.
35. Hatanaka, M., Hu, J. G., Petkova, A. T., Bizounok, M., Verhoeven, M., Lugtenburg, J., Griffin, R. G., and Herzfeld, J. (1999) *Biophys. J. 76*, A241 (abstract).
36. Towner, P., Gärtner, W., Walckhoff, B., Oesterhelt, D., and Hopf, H. (1981) *Eur. J. Biochem. 117*, 353−359.
37. Pardoen, J. A., Winkel, C., Mulder, P. P. J., and Lugtenburg, J. (1984) *Rec. Trav. Chim. Pays-Bas 103*, 135−141.
38. Oesterhelt, D., and Krippahl, G. (1983) *Ann. Microbiol. 134B*, 137−150.
39. Gullion, T., and Schaefer, J. (1989) *J. Magn. Reson., Ser. B 81*, 196−200.
40. Drobny, G., Pines, A., Sinton, S., Weitkamp, D., and Wemmer, D. (1979) *Faraday Div. Chem. Soc. Symp. 13*, 49.
41. Bodenhausen, G., Vold, R. L., and Vold, R. R. (1980) *J. Magn. Reson. 37*, 93−106.
42. Mueller, K. T. (1995) *J. Magn. Reson., Ser. A 113*, 81−93.
43. Goetz, J. M., and Schaefer, J. (1997) *J. Magn. Reson. 127*, 147−154.
44. Harbison, G. S., Smith, S. O., Pardoen, J. A., Mulder, P. P., Lugtenburg, J., Herzfeld, J., Mathies, R., and Griffin, R. G. (1984) *Biochemistry 23*, 2662−2667.
45. Scherrer, P., Mathew, M. K., Sperling, W., and Stoeckenius, W. (1989) *Biochemistry 28*, 829−834.
46. Cotten, M., Fu, R., and Cross, T. A. (1999) *Biophys. J. 76*, 1179−1189.
47. de Groot, H. J., Harbison, G. S., Herzfeld, J., and Griffin, R. G. (1989) *Biochemistry 28*, 3346−3353.
48. Hildebrandt, P., and Stockburger, M. (1984) *Biochemistry 23*, 5539−5548.
49. Harbison, G. S., Roberts, J. D., Herzfeld, J., and Griffin, R. G. (1988) *J. Am. Chem. Soc. 110*, 7221.
50. Metz, G., Siebert, F., and Engelhard, M. (1992) *Biochemistry 31*, 455−462.
51. Steinmuller, S., Buss, V., and Gartner, W. (1995) *J. Photochem. Photobiol. B 31*, 139−144.
52. Smith, S. O., de Groot, H. J., Gebhard, R., Courtin, J. M., Lugtenburg, J., Herzfeld, J., and Griffin, R. G. (1989) *Biochemistry 28*, 8897−8904.

BI0006666